V International Conference on Computational Methods for Coupled Problems in Science and Engineering
COUPLED PROBLEMS 2013
S. Idelsohn, M. Papadrakakis and B. Schrefler (Eds)

WIND TURBINE SIMULATION: STRUCTURAL MECHANICS, FSI AND COMPUTATIONAL STEERING

Y. BAZILEVS[*], A. KOROBENKO[*], X. DENG[*], J. TIPPMANN[*] AND M.-C. HSU[†]

[*] Department of Structural Engineering
University of California, San Diego
La Jolla, CA 92093, USA

[†]Institute for Computational Engineering and Sciences
The University of Texas at Austin
201 E. 24th St. Stop C0200
Austin, TX 78712, USA

Key words: Fluid–structure interaction, nonmatching interface discretization, isogeometric analysis, composite materials, wind turbine, wind turbine blade, ALE-VMS, rotor-tower interaction, KirchhoffLove shells, DDDAS, fiber waviness

Abstract. A fluid-structure interaction (FSI) validation study of Micon 65/13M wind turbine with Sandia CX-100 composite blades is presented. KirchhoffLove shell theory is used for blade structures, while the aerodynamics formulation is performed using a moving-domain finite-element-based ALE-VMS technique. The structural mechanics formulation is validated through the eigenfrequency analysis of the CX-100 blade. For coupling between two domains a nonmatching discretization of the fluid-structure interface is adopted. This adds flexibility and relaxes the requirements placed on geometry modeling and meshing tools employed. The simulations are done at realistic wind conditions and rotor speeds. The rotor-tower interaction that influences the aerodynamic torque is captured. The computed aerodynamic torque generated by the Micon 65/13M wind turbine compares well with that obtained from on-land field tests. We conclude by illustrating the application of the Dynamic Data-Driven Applications System (DDDAS) to investigate the fiber waviness defects embedded in the CX-100 wind turbine blade.

1 INTRODUCTION

In modern computational analysis of wind turbines, FSI simulations at full scale are important for accurate and reliable modeling, as well as blade failure prediction and design optimization. The wind turbine FSI problem presents significant computational challenges because of the curved geometry of the wind turbine blades, complex distribution of material properties, wind and rotor speeds that lead to complex, wall-bounded turbulent flows, and the presence of mechanical components in relative motion. Because of the challenges involved in the aerodynamics modeling, only a handful of researchers (see, e.g., [15, 17, 24, 34]) performed wind turbine simulations at full scale and with all the turbine components (i.e. blades, tower and nacelle) included. The fully coupled FSI simulations of full-scale wind turbine designs were performed only recently in [1] for the rotor-only case and in [18] for the full machine.

In this paper we present the structural, aerodynamic, and FSI simulations of the Sandia CX-100 blade. Most of the methods and results resented here may be found in [23]. The FSI framework developed in [2] is adopted wherein isogeometric analysis (IGA) [13, 19] is employed for structural mechanics. The aerodynamics formulation makes use of a finite-element-based ALE-VMS technique [9]. The sliding interface formulation developed in [5] employed in conjunction with the ALE-VMS technique [3] enables the simulation of the interaction between the spinning rotor and stationary tower. In addition, for improved boundary-layer accuracy, a key ingredient employed in the ALE-VMS simulation of wind-turbine aerodynamics and FSI are the weakly enforced no-slip boundary conditions [4, 7, 8] set on the moving blade surfaces.

The blade structures are modeled using the rotation-free multilayer composite Kirchhoff–Love shell [1, 21, 22]. Prior to using this blade in our FSI computation, we perform its eigenfrequency analysis and compare the results with the experimental data. This presents the first validation of the rotation-free Kirchhoff–Love IGA shell for a full-scale wind turbine blade. In addition to eigenfrequency analysis, we use the same isogeometric model of the CX-100 blade for the structural mechanics simulations in the context of the Dynamic Data-Driven Applications System (DDDAS) framework [14]. In particular, we focus on in-plane fiber waviness defects, which are typical for multi-layer composite structures, and show how to incorporate such defects, coming from sensor data, into the isogeometric model of the blade.

2 NUMERICAL METHODS AND RESULTS

To show the accuracy and reliability of the presented FSI framework, simulations of the Micon 65/13M wind turbine are carried out at realistic operational conditions, reported in [35]. The turbine is designed as a three-blade, fixed-pitch, upwind turbine with the total rotor diameter of 19.3 m and rated power of 100 kW. The hub is located at the height of 23 m, with a mounting flange positioned 0.6 m from the centerline of the low speed shaft. The wind turbine stands on a tubular steel tower, with a base diameter of 1.9 m. The drive train generator operates at 1200 rpm, while the rotor spins at a nominal speed of 55 rpm. The Micon 65/13M wind turbine was used for the Long-Term Inflow and Structural Testing (LIST) program [27] at the USDA-ARS test facility in Bushland, Texas. This project was initiated by Sandia National Lab-

oratories in 2001 to explore the use of carbon fiber in wind turbine blades. Three experimental blade prototypes, GX-100, CX-100 and TX-100, were developed specifically for this project.

2.1 Structural mechanics

For the simulation of the Micon 65/13M wind turbine, we make use of the Sandia CX-100 carbon-spar blade [12, 35] which is an actual design that has over 32 material zones with complex, nonsymmetric composite layup in each zone (see Figure 1). To model the blade, including the full composite layup, we use a rotation-free Kirchhoff–Love shell formulation [22] discretized using NURBS-based IGA [13, 19]. The Kirchhoff–Love formulation is augmented with the bending strip method proposed in [21].

We perform eigenfrequency calculations of the CX-100 blade using three quadratic NURBS meshes. The coarsest mesh has 1,846 elements, while the nest mesh has 18,611 elements. The mesh statistics are summarized in Table 1. The eigenfrequency results are compared with the experimental data from [25, 33]. We compute the case with free boundary conditions and the case when the blade is clamped at the root. For the free case the eigenfrequencies for the first and second flapwise bending modes and for the first edgewise bending mode are summarized in Table 2. The experimental eigenfrequencies are obtained for this blade at Sandia National Laboratories (SNL), Los Alamos National Laboratory (LANL) and the University of Massachusetts Lowell Structural Dynamics and Acoustics Laboratory (UML SDASL), and reported in [25].

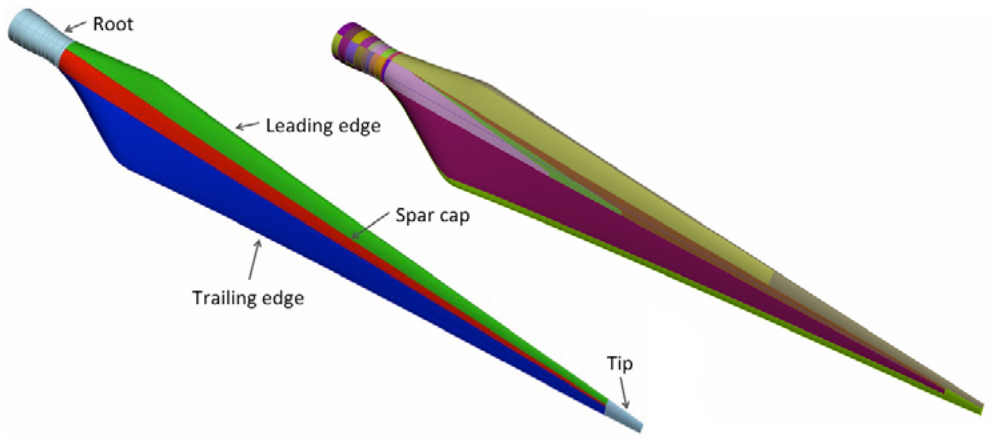

Figure 1: Left: Five primary sections of the CX-100 blade; Right: 32 distinct material zones of the CX-100 blade.

	Number of Control Points	Number of Elements
Mesh 1	3,469	1,846
Mesh 2	7,411	4,647
Mesh 3	25,896	18,611

Table 1: NURBS blade meshes used in the eigenfrequency analysis.

Mode:	1^{st} Flapwise (Hz)	1^{st} Edgewise (Hz)	2^{nd} Flapwise (Hz)
Mesh 1	8.28	15.92	19.26
Mesh 2	8.22	15.61	18.21
Mesh 3	8.22	15.6	18.01
Experiment	7.6 - 8.2	15.7 - 18.1	20.2 - 21.3

Table 2: Comparison of experimentally measured and computed natural frequencies corresponding to the first few bending modes for the free case.

Mode:	1^{st} Flapwise (Hz)	2^{nd} Flapwise (Hz)	3^{rd} Flapwise (Hz)
Mesh 1	4.33	11.82	19.69
Mesh 2	4.29	11.61	19.08
Mesh 3	4.27	11.54	18.98
Experiment	4.35	11.51	20.54

Table 3: Comparison of experimentally measured and computed natural frequencies corresponding to the first few bending modes for the clamped case.

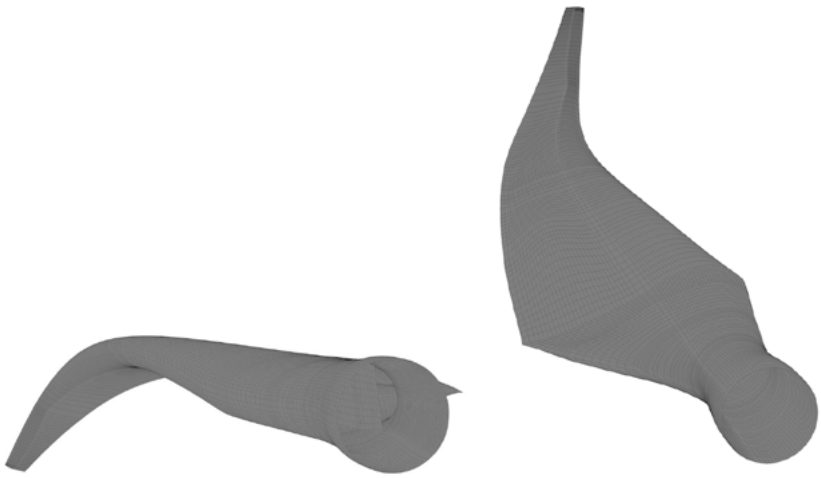

(a) (b)

Figure 2: First flapwise bending mode (a) and first edgewise bending mode (b), for the free case.

Table 2 provides a range of experimental eigenfrequency values. For the clamped case, the eigenfrequencies for the first three bending modes are compared with the results of the tests performed at the National Renewable Energy Laboratory (NREL) [25]. In both cases, the computed natural frequencies are in good agreement with the experimental data (see Table 3). The medium mesh shows a good balance between the computational cost and accuracy of the results. For this reason, this mesh is chosen for the FSI computations presented in the next section. The mode shapes computed using the medium mesh are shown in Figures 2 and 3.

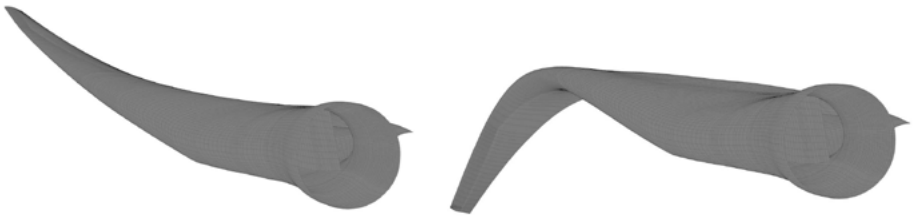

(a) (b)

Figure 3: First flapwise bending mode (a) and second flapwise bending mode (b), for the clamped case.

2.2 Aerodynamics and FSI

The wind turbine aerodynamics is governed by the Navier–Stokes equations of incompressible flows. The incompressible-flow assumption is valid for the present application because the Mach number is low. The aerodynamics formulation makes use of the FEM-based ALE-VMS approach [3] augmented with weakly enforced boundary conditions [4]. The former acts as a turbulence model, while the latter relaxes the mesh size requirements in the boundary layer without sacrificing the solution accuracy. The framework includes FSI modeling with nonmatching discretization of the interface between the fluid and structure subdomains. We take advantage of the flexibility associated with using nonmatching discretizations, combining the most appropriate discretization for each part of an FSI problem. The use of nonmatching grids also allows for adopting different geometry modeling and meshing tools for the fluid and structural mechanics subproblems. Nonmatching discretizations at the fluidstructure interface require the use of interpolation or projection of kinematic and traction data between the nonmatching surface meshes (see, for example, [2, 28, 29]), and that is what we do here.

To simulate the full machine, we use a sliding-interface formulation developed in [5], and recently employed for wind-turbine simulations in [17, 18]. We note that in application of the FEM to flows with moving mechanical components, the Shear–Slip Mesh Update Method [10, 11, 30] and its more general versions [31, 32] may also be used to handle objects in relative motion.

An aerodynamic and FSI simulations of the full Micon 65/13M wind turbine are presented for a constant inflow wind speed of 10.5 m/s and fixed rotor speed of 55 rpm are prescribed. These correspond to the operating conditions reported for the field tests in [35]. The air density and viscosity are set to 1.23 kg/m^3 and 1.78×10^{-5} kg/(m·s), respectively.

The computations were carried out in a parallel computing environment. The meshes, which consist of linear triangular prisms in the boundary layers and linear tetrahedra elsewhere, are partitioned into subdomains using METIS [20], and each subdomain is assigned to a compute core. The parallel implementation of the methodology may be found in [16]. The time step is set to 3.0×10^{-5} s for all cases.

In Figure 4 the time history of the aerodynamic torque is plotted. As can be seen from the plot, using FSI, we capture the high frequency oscillations caused by the bending and torsional motions of the blades. In the case of the rigid blade the only high-frequency oscillations in

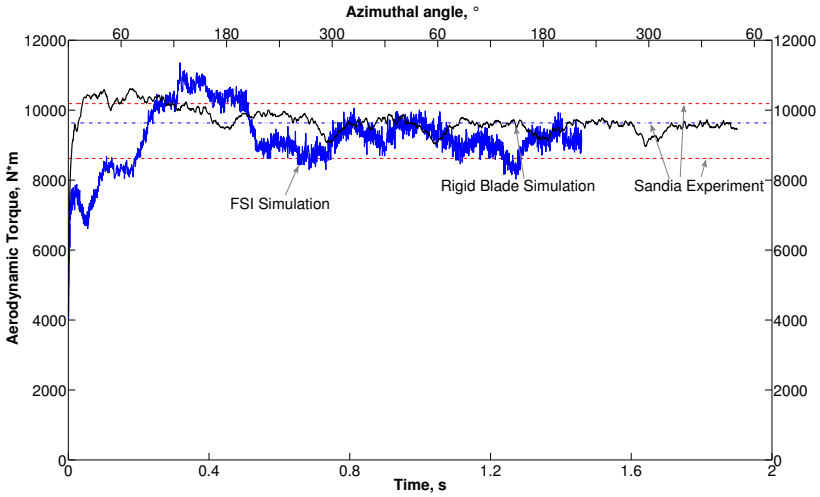

Figure 4: Aerodynamic torque history for the FSI and rigid-blade simulations. The experimental range for the aerodynamic torque and its average value are provided for comparison and are plotted using dashed lines.

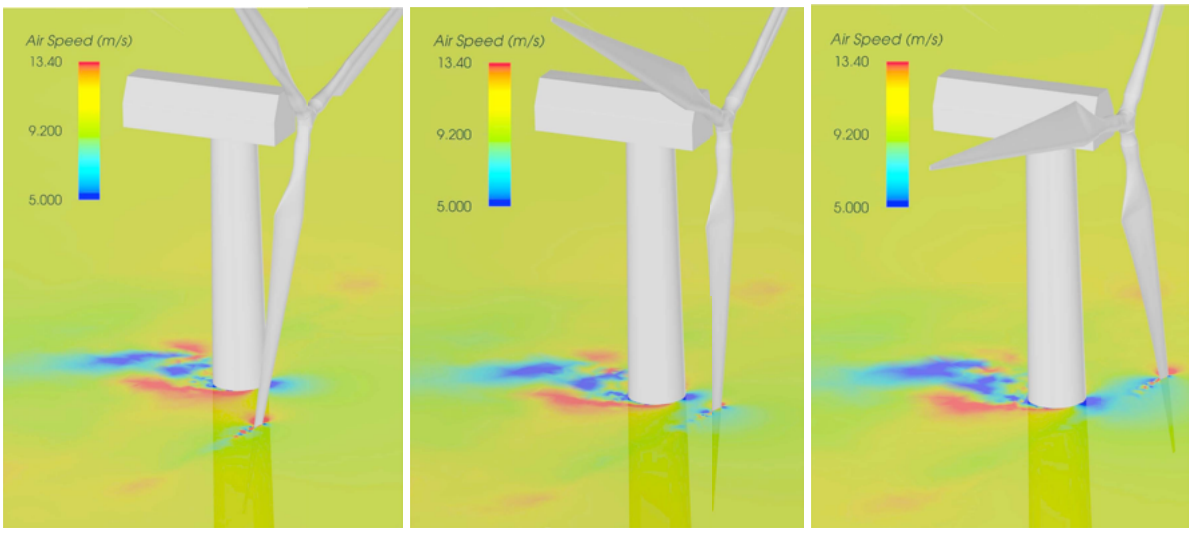

Figure 5: Wind speed contours at 80% spanwise station as the blade passes the tower.

the torque curve are due to the trailing-edge turbulence. For the rigid blade case the effect of the tower on the aerodynamic torque is more pronounced, while in the case of FSI it is not as visible due to the relatively high torque oscillations. The 'dips' in the aerodynamic torque can be seen at 60°, 180°, and 300° azimuthal angle, which is precisely when one of the three blades is passing the tower.

The computed values of the aerodynamic torque are plotted together with field test results from [35]. The upper and lower dashed lines indicate the aerodynamic torque bounds, while the middle dashed line gives its average value. Both the aerodynamic and FSI results compare very

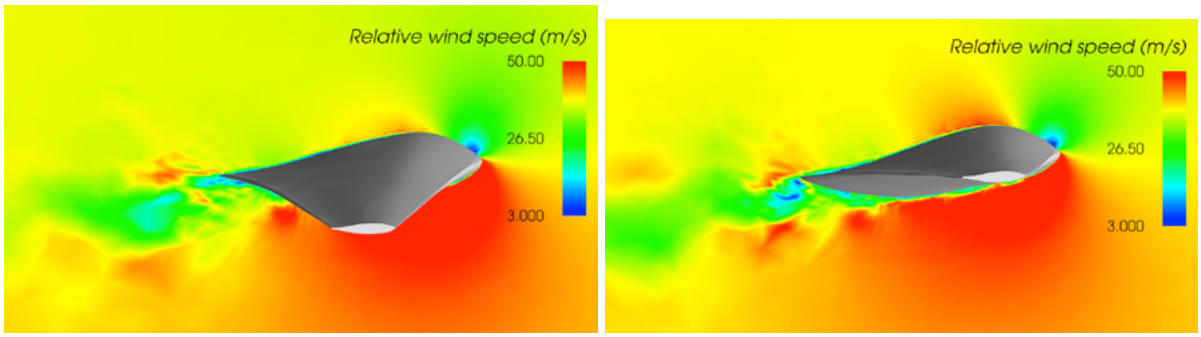

Figure 6: Relative wind speed at the 70% spanwise station for the FSI simulation at $t = 0.86$ s (left) and $t = 1.06$ s (right). The blade deflection is clearly visible.

well with the experimental data.

Figure 5 shows the flow field as the blade passes the tower. Figure 6 shows the relative wind speed at the 70% spanwise station rotated to the reference configuration to illustrate the blade deflection and complexity of boundary-layer turbulent flow.

2.3 DDDAS

DDDAS is a framework in which measurement data collected for a given physical system are used to dynamically update a computational model of that system. Using measurement data, the computational model geometry, boundary conditions, forcing, and material parameters may be updated to better represent physical reality. At the same time, the properly updated computational model is able to produce higher-fidelity outputs for the quantities of interest for which measurements are not readily available. As such, DDDAS is a framework in which measurement and simulation co-exist in a symbiotic environment. Many applications of DDDAS involve not only updating of the computational model on the basis of sensor data, but also adjustment of the model and physical system input parameters to optimize a desired outcome. For example, in [26], the authors developed and deployed a DDDAS framework for computational steering of the laser-guided surgery for prostate cancer treatment. The temperature and location of the laser were dynamically controlled to achieve maximum damage to the cancerous tissue.

In our case, we are interested in a DDDAS framework for large-scale structures exposed to aerodynamic loading [6]. One of the main features of the framework proposed in [6] is the use of IGA to model shell structures made of laminated composites. The use of a single geometry for modeling and simulation, which is one of the tenets of IGA, has several benefits for DDDAS. Here we take advantage of the parametric description of the blade geometry in order to locate the composite fiber waviness defect (detected by the sensors) on the model surface, and to impose the fiber waviness during the through-thickness homogenization process. Because fiber waviness is a local phenomenon, the computational mesh needs to be refined in order to capture the local variation in the strain (and stress) components. Schematic of the DDDAS modeling applied in the context of composite fiber waviness defects is illustrated in Figure 7. The more general DDDAS procedure may be described as a feedback loop, which

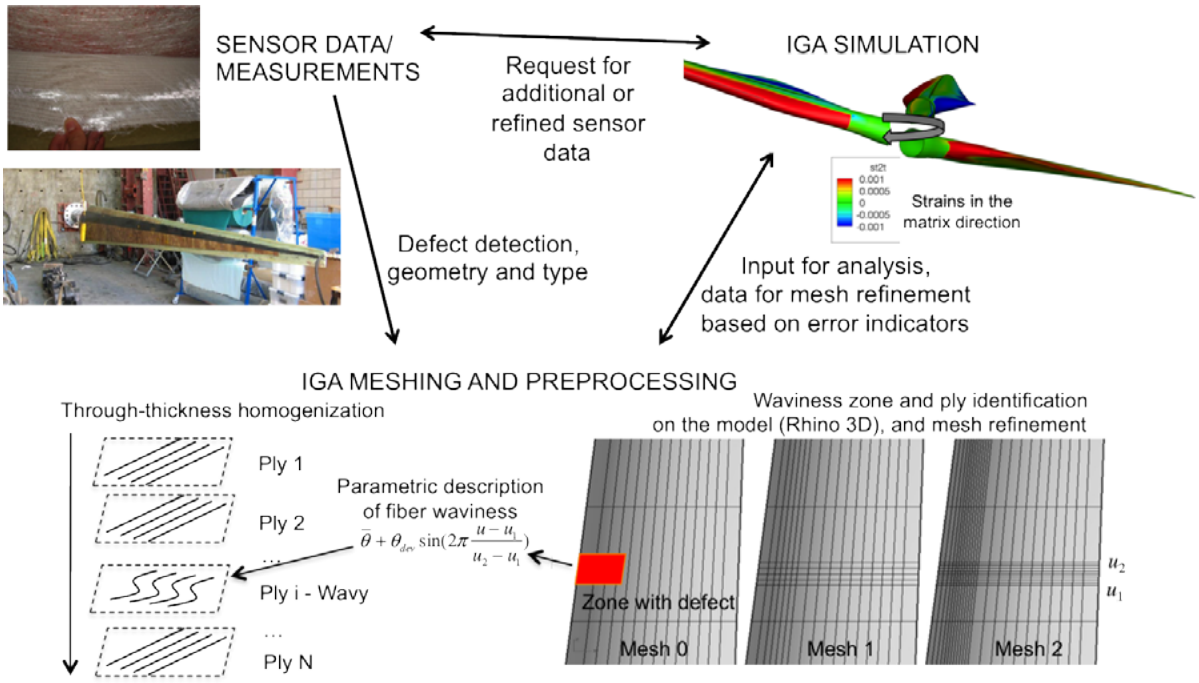

Figure 7: DDDAS loop for in-plane fiber waviness.

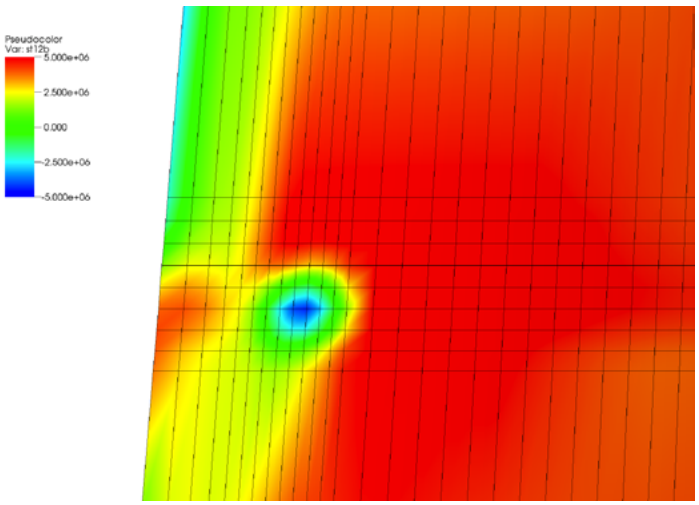

Figure 8: Local mesh refinement that captured in-plane shear stress variation due to the detected in-plane fiber waviness.

contains the actual structure with embedded sensors that provide feedback to the simulation and modeling/meshing modules. The concentration of the in-plane shear strain after the defect was located and the mesh was refined locally is shown in Figure 8.

3 CONCLUSIONS

We constructed a detailed structural model of the actual wind turbine blade, which has 32 material zones. Each of the material zones was characterized with its distinct composite layup. Nonsymmetric layup was used in all zones, which introduced coupling between the membrane and bending response of the Kirchhoff–Love shell. Despite the discontinuity in the material properties, almost everywhere C^1-continuous quadratic NURBS basis was used to discretize the shell kinematics, and the NURBS mesh lines were not aligned with the boundaries of the material zones. The material properties were approximated at the quadrature points of the NURBS mesh. With this construction, we were able to reproduce the experimentally measured eigenfrequencies of the CX-100 blade. To our knowledge, this is the first full-scale validation of the IGA-based thin-shell composite formulation..

We used the previously developed ALE-VMS formulation for modeling the turbulent flow, FSI coupling of FEM and IGA, weakly enforced boundary conditions, and a sliding interface formulation to compute the full Micon 65/13M wind turbine with the CX-100 blades mounted on its rotor. The results of the aerodynamic and FSI simulations are in a good agreement with field test data for this wind turbine. The FSI simulation captures high-frequency oscillations in the aerodynamic torque, which are caused by the blade structural response.

Finally, we illustrated the benefits of using IGA within a recently proposed DDDAS framework for in-plane fiber waviness calculations in composites.

ACKNOWLEDGEMENTS

The support of the AFOSR Award No. FA9550-12-1-0005 is gratefully acknowledged. X. Deng was supported through AFOSR Award No. FA9550-12-1-0046. We thank the Sandia National Laboratories Wind Energy Technologies program for providing us access to the data, which enabled the construction of the wind turbine blade structural model. We also thank the Texas Advanced Computing Center (TACC) at the University of Texas at Austin and the San Diego Supercomputing Center (SDSC) at the University of California, San Diego for providing HPC resources that have contributed to the research results reported in this paper.

REFERENCES

[1] Y. Bazilevs, M.-C. Hsu, J. Kiendl, R. Wüchner, and K.-U. Bletzinger. 3D simulation of wind turbine rotors at full scale. Part II: Fluid–structure interaction modeling with composite blades. *International Journal for Numerical Methods in Fluids*, 65:236–253, 2011.

[2] Y. Bazilevs, M.-C. Hsu, and M. A. Scott. Isogeometric fluid–structure interaction analysis with emphasis on non-matching discretizations, and with application to wind turbines. *Computer Methods in Applied Mechanics and Engineering*, 249-252:28–41, 2012. doi:10.1016/j.cma.2012.03.028.

[3] Y. Bazilevs, M.-C. Hsu, K. Takizawa, and T.E. Tezduyar. ALE-VMS and ST-VMS methods for computer modeling of wind-turbine rotor aerodynamics and fluid–structure interaction. *Mathematical Models and Methods in Applied Sciences*, 22:1230002, 2012.

[4] Y. Bazilevs and T. J. R. Hughes. Weak imposition of Dirichlet boundary conditions in fluid mechanics. *Computers and Fluids*, 36:12–26, 2007.

[5] Y. Bazilevs and T. J. R. Hughes. NURBS-based isogeometric analysis for the computation of flows about rotating components. *Computational Mechanics*, 43:143–150, 2008.

[6] Y. Bazilevs, A.L. Marsden, F. Lanza di Scalea, A. Majumdar, and M. Tatineni. Toward a computational steering framework for large-scale composite structures based on continually and dynamically injected sensor data. *Procedia Computer Science*, 9:1149–1158, 2012.

[7] Y. Bazilevs, C. Michler, V. M. Calo, and T. J. R. Hughes. Weak Dirichlet boundary conditions for wall-bounded turbulent flows. *Computer Methods in Applied Mechanics and Engineering*, 196:4853–4862, 2007.

[8] Y. Bazilevs, C. Michler, V. M. Calo, and T. J. R. Hughes. Isogeometric variational multiscale modeling of wall-bounded turbulent flows with weakly enforced boundary conditions on unstretched meshes. *Computer Methods in Applied Mechanics and Engineering*, 199:780–790, 2010.

[9] Y. Bazilevs, K. Takizawa, and T.E. Tezduyar. *Computational Fluid–Structure Interaction: Methods and Applications*. Wiley, Chichester, 2013.

[10] M. Behr and T. Tezduyar. The Shear-Slip Mesh Update Method. *Computer Methods in Applied Mechanics and Engineering*, 174:261–274, 1999.

[11] M. Behr and T. Tezduyar. Shear-slip mesh update in 3D computation of complex flow problems with rotating mechanical components. *Computer Methods in Applied Mechanics and Engineering*, 190:3189–3200, 2001.

[12] D. Berry and T. Ashwill. Design of 9-meter carbon-fiberglass prototype blades: CX-100 and TX-100. 2007. Report of the Sandia National Laboratories.

[13] J. A. Cottrell, T. J. R. Hughes, and Y. Bazilevs. *Isogeometric Analysis: Toward Integration of CAD and FEA*. Wiley, Chichester, 2009.

[14] F. Darema. Dynamic data driven applications systems: A new paradigm for application simulations and measurements. *Proceedings of ICCS 2004 4th International Conference on Computational Science*, pages 662–669, 2004.

[15] S. Gómez-Iradi, R. Steijl, and G. N. Barakos. Development and validation of a CFD technique for the aerodynamic analysis of HAWT. *Journal of Solar Energy Engineering*, 131:031009–1–13, 2009.

[16] M.-C. Hsu, I. Akkerman, and Y. Bazilevs. High-performance computing of wind turbine aerodynamics using isogeometric analysis. *Computers & Fluids*, 49:93–100, 2011.

[17] M.-C. Hsu, I. Akkerman, and Y. Bazilevs. Finite element simulation of wind turbine aerodynamics: Validation study using NREL Phase VI experiment. *Wind Energy*, 2013. Accepted.

[18] M.-C. Hsu and Y. Bazilevs. Fluid–structure interaction modeling of wind turbines: Simulating the full machine. *Computational Mechanics*, 50:821–833, 2012.

[19] T. J. R. Hughes, J. A. Cottrell, and Y. Bazilevs. Isogeometric analysis: CAD, finite elements, NURBS, exact geometry, and mesh refinement. *Computer Methods in Applied Mechanics and Engineering*, 194:4135–4195, 2005.

[20] G. Karypis and V. Kumar. A fast and high quality multilevel scheme for partitioning irregular graphs. *SIAM Journal on Scientific Computing*, 20:359–392, 1999.

[21] J. Kiendl, Y. Bazilevs, M.-C. Hsu, R. Wüchner, and K.-U. Bletzinger. The bending strip method for isogeometric analysis of Kirchhoff–Love shell structures comprised of multiple patches. *Computer Methods in Applied Mechanics and Engineering*, 199:2403–2416, 2010.

[22] J. Kiendl, K.-U. Bletzinger, J. Linhard, and R. Wüchner. Isogeometric shell analysis with Kirchhoff–Love elements. *Computer Methods in Applied Mechanics and Engineering*, 198:3902–3914, 2009.

[23] A. Korobenko, M.-C. Hsu, I. Akkerman, J. Tippmann, and Y. Bazilevs. Structural mechanics modeling and FSI simulation of wind turbines. *Mathematical Models and Methods in Applied Science*, 23:249–272, 2013. DOI: 10.1142/S0218202513400034.

[24] Y. Li and P. M. Carrica K. J. Paik, T. Xing. Dynamic overset CFD simulations of wind turbine aerodynamics. *Renewable Energy*, 37:285–298, 2012.

[25] T. Marinone, B. LeBlanc, J. Harvie, C. Niezrecki, and P. Avitabile. Modal testing of a 9 m CX-100 turbine blades. pages Topics in Experimental Dynamics Substructuring and Wind Turbine Dynamics, Volume 2, Conference Proceedings of the Society for Experimental Mechanics Series 27, 2012.

[26] J.T. Oden, K.R. Diller, C. Bajaj, J.C. Browne, J. Hazle, I. Babuska, J. Bass, L. Demkowicz, Y. Feng, D. Fuentes, S. Prudhomme, M.N. Rylander, R.J. Stafford, and Y. Zhang. Dynamic data-driven finite element models for laser treatment of prostate cancer. *Num. Meth. PDE*, 23(4):904–922, 2007.

[27] J. H. Sutherland, P. L. Jones, and B.A. Neal. The long-term inflow and structural test program. 2001. Proceedings of the 2001 ASME Wind Energy Symposium, p.162.

[28] K. Takizawa and T. E. Tezduyar. Multiscale space–time fluid–structure interaction techniques. *Computational Mechanics*, 48:247–267, 2011.

[29] K. Takizawa and T.E. Tezduyar. Space–time fluid–structure interaction methods. *Mathematical Models and Methods in Applied Sciences*, 22:1230001, 2012.

[30] T. Tezduyar, S. Aliabadi, M. Behr, A. Johnson, V. Kalro, and M. Litke. Flow simulation and high performance computing. *Computational Mechanics*, 18:397–412, 1996.

[31] T. E. Tezduyar. Finite element methods for flow problems with moving boundaries and interfaces. *Archives of Computational Methods in Engineering*, 8:83–130, 2001.

[32] T. E. Tezduyar. Finite elements in fluids: Special methods and enhanced solution techniques. *Computers & Fluids*, 36:207–223, 2007.

[33] J.R. White, D.E. Adams, and M.A.Rumsey. Modal analysis of CX-100 rotor blade and Micon 65/13 wind turbine. pages Structural Dynamics and Renewable Energy, Volume 1, Conference Proceedings of the Society for Experimental Mechanics Series 10, 2011.

[34] F. Zahle, N. N. Sørensen, and J. Johansen. Wind turbine rotor-tower interaction using an incompressible overset grid method. *Wind Energy*, 12:594–619, 2009.

[35] J.R. Zayas and W.D. Johnson. 3X-100 blade field test. *Wind Energy Technology Department, Sandia National Laboratories*, page Report, 2008.